AREVA

ANP-10340NP
Revision 0

Incorporation of Chromia-Doped Fuel Properties in AREVA Approved Methods

Topical Report

April 2016

AREVA Inc.

Nature of Changes

Item	Revision Number	Section(s) or Page(s)	Description and Justification
1.	0	All	This is the initial release.

Contents

List of Tables

List of Figures

This document contains a total of 118 pages.

Nomenclature

Acronym	Definition
AOO	Anticipated Operational Occurrence
BWR	Boiling Water Reactor
CEA	Commissariat a l'Energie Atomique
CPR	Critical Power Ratio
CRDA	Control Rod Drop Accident
CRWE	Control Rod Withdrawal Error
CWSR	Cold-Worked Stress-Relieved
FDL	Fuel Design Limit
FGR	Fission Gas Release
HBS	High Burnup Structure
JRC-ITU	Joint Research Centre – Institute for Transuranium Elements
LFA	Lead Fuel Assembly
LHGR	Linear Heat Generation Rate
LOCA	Loss of Coolant Accident
LWR	Light Water Reactor
MLI	Mean Linear Intercept
PCI	Pellet-Cladding Interaction
PCMI	Pellet-Cladding Mechanical Interaction
PCT	Peak Cladding Temperature
PIE	Post-Irradiation Examination
PWR	Pressurized Water Reactor
RIA	Reactivity Initiated Accident
RTL	Ramp Terminal Level
RXA	Recrystallized Annealed
TD	Theoretical Density

ABSTRACT

AREVA has developed chromia-doped fuel by adding a small quantity of chromia (Cr_2O_3) to standard fuel. This doped fuel is similar to standard fuel, but the chromia dopant greatly enhances grain growth during sintering; and therefore, chromia-doped fuel is characterized by larger grain size than standard fuel. This topical report examines the effect of the use of chromia-doped fuel and its implementation in AREVA methodology.

A discussion is presented of the applicable regulatory guidance related to fuel material. This guidance is found primarily in NUREG-0800 Sections 4.2 through 4.4. The effects the incorporation of chromia-doped fuel has on the methods which support the applicable NUREG-0800 criteria are provided.

The material properties and behavioral aspects of the chromia-doped fuel in comparison to standard fuel are described. Chromia-doped fuel is similar to standard fuel and the few properties that differ are identified. The available chromia-doped fuel database of both separate-effects and integral tests that can be used for fuel model qualification is presented. While the qualification database, material, and behavioral sections of this report are valid for both BWR and PWR applications, the model adaptation to chromia-doped fuel is code specific.

A description of how AREVA's BWR codes have been modified and validated to support the use of chromia-doped fuel is provided. Code adjustments were made to accommodate changes in the thermal conductivity and gaseous swelling models. No other changes to any of the current BWR methodologies were necessary.

The adaptation and qualification of RODEX4 and S-RELAP5 to chromia-doped fuel is presented. Sample cases of design analyses are provided that cover the entire range for fuel licensing under RODEX4-based BWR methodologies for thermal-mechanical analyses, thermal limits and safety analyses.

Finally, the report summarizes AREVA's experience with chromia-doped fuel for both steady state irradiation and ramp testing, and demonstrates the chromia-doped fuel benefit with respect to reduced fuel failure.

1.0 INTRODUCTION

AREVA has developed chromia-doped fuel by adding a small quantity of chromia (Cr_2O_3) to standard fuel. This doped fuel is similar to standard fuel, but the chromia dopant greatly enhances grain growth during sintering; and therefore, chromia-doped fuel is characterized by larger grain size than standard fuel. This results in a reduction of fission gas release and also a diminished potential for fuel washout from a failed fuel rod. At the same time, chromia-doped fuel has improved behavior during power transients, which is translated into higher pellet-cladding interaction (PCI) failure thresholds in comparison with standard fuel.

The benefits of chromia-doped fuel are relevant to both BWR and PWR fuel rods and in each type of reactor conditions. While the qualification database, material, and behavioral sections of this report are valid for both BWR and PWR applications, the model adaptation to chromia-doped fuel is code specific.

BWR fuel methods are addressed by describing the qualification of the RODEX4 fuel code for chromia-doped fuel, together with the related upstream and downstream codes and methods. BWR fuel rod growth is the one performance characteristic affected by chromia-doped fuel that is not addressed within this report. Fuel rod growth will be addressed in a separate topical report for NRC approval prior to licensing of BWR chromia-doped fuel.

2.0 SUMMARY

This report provides a description of the changes to AREVA's RODEX4 fuel code and its validation in order to support the use of chromia-doped BWR fuel. In addition the upstream neutronics codes and methods and the downstream thermal-hydraulic codes and methods have been analyzed for any needed adaptation to chromia-doped fuel. No adaptation was identified for the neutronics codes and methods, while an update of the thermal conductivity model for the S-RELAP5 code was identified for the downstream thermal-hydraulic codes and methods.

The report provides the material properties of chromia-doped fuel in Section 4.0 with the associated qualification dataset, which provides the basis for properties that are different from those of standard fuel. For the material properties that are not affected by the chromia dopant, experimental and/or theoretical justification is provided to support the continued use of the material property for chromia-doped fuel.

Section 5.0 describes the chromia-doped fuel characteristics that are related to in-reactor behavior during normal operation, accident conditions, and following fuel failure.

The validation and verification (i.e. qualification) database that is required in order to qualify a fuel code for chromia-doped applications is described in Section 6.0. This data is presented in Section 7.0. Measurements taken on fuel rods during and after irradiation testing are used in combination with separate-effects testing to provide data to characterize material properties.

Sections 7.0 through 9.0 describe how the general properties of chromia-doped fuel are modeled in the AREVA RODEX4-based BWR methodology to generate sample licensing evaluations in support of typical core designs. The adaptation and qualification of RODEX4 to chromia-doped fuel are described in Section 7.0. The qualification of RODEX4 to chromia-doped fuel also justifies the removal of the grain size restriction imposed in the Safety Evaluation for Reference 20. Section 8.0 provides information regarding qualification of the AURORA-B S-RELAP5 models for chromia-doped fuel. Finally, for illustration purposes, Section 9.0 presents sample cases of

design analyses that cover the full range of calculations for fuel licensing under RODEX4-based BWR methodologies to demonstrate compliance with the licensing criteria which are discussed in Section 3.0.

The operating experience with chromia-doped fuel in power reactors is contained in Section 10.0. This section also describes the comprehensive power ramp program that is the basis for the quantification of the PCI performance improvement with chromia-doped fuel.

3.0 APPLICABLE REGULATORY GUIDANCE

Regulatory guidance for the review of fuel system designs and adherence to applicable General Design Criteria is provided in NUREG-0800, "Standard Review Plan for the Review of Safety Analysis Reports for Nuclear Power Plants", Section 4.2, "Fuel System Design" (Reference 1).

The SRP Section 4.3 is not discussed in this report because there are no changes required for the application of the neutronics codes and methods to chromia-doped fuel. Chromium neutron cross-sections are present in the lattice codes, and the neutronics methods accurately model this element as described in Section 9.3 of this report.

The SRP Section 4.4, which refers to the thermal and hydraulic design, is also not impacted by the chromia-doped fuel because the small change to fuel composition has no effect on any of the processes and phenomena related to thermal and hydraulic design of the core. However, the results of the analyses required by SRP Section 4.2 (which are also cross-referenced in SRP Section 4.4) are slightly modified by the specific properties of chromia-doped fuel. Therefore, the corresponding design basis topics are included in the following discussion of compliance with the applicable regulatory guidance.

In accordance with the Standard Review Plan Section 4.2, the objectives of the fuel system safety review are to provide assurance that:

- The fuel system is not damaged as a result of normal operation and anticipated operational occurrences (AOOs).
- Fuel system damage is never so severe as to prevent control rod insertion when it is required.
- The number of fuel rod failures is not underestimated for postulated accidents, and
- Fuel coolability is always maintained.

As there is no change to cladding materials or fuel assembly design and structural materials, only the Standard Review Plan fuel design criteria from Section 4.2 that are germane to implementation of chromia-doped fuel are described in Table 3-1. The only exception is the fuel rod growth model which is not addressed in this report. It is more appropriate to address fuel rod growth in the fuel mechanical topical report to be consistent with the suite of current AREVA BWR methods.

SRP Chapter 15 acceptance criteria for AOOs and accidents are addressed in Section 9.2, where representative events are analyzed and the effect of employing chromia-doped fuel on margins to acceptance criteria limits are evaluated. Table 3-1 addresses the SRP Chapter 15 acceptance criteria for the Section 4.2 design criteria that apply.

Data is provided in this topical report to allow removal of the grain size restriction imposed in the Safety Evaluation for Reference 20. The removal of this restriction is needed due to the larger grain size of chromia-doped fuel.

Table 3-1 Standard Review Plan Section 4.2 Criteria

1. Design Bases	Item	Topic	Assessment	Location in this Report
A. Fuel System Damage	i	Stress, strain, or loading limits (fuel rod cladding)	[ ]	See row B.vi of this table for information on cladding strain.
	ii	Fatigue (fuel rod cladding)	[ ]	Section 9.1 provides analysis results.
	iii	Fretting wear (fuel rod cladding)	[ ]	Since neither the method nor calculated results are affected by the use of chromia-doped fuel, this topic is not included in the report.
	iv	Oxidation, hydriding, crud (fuel rod cladding)	[ ]	Since neither the method nor calculated results are affected by the use of chromia-doped fuel, this topic is not included in the report.
	v	Dimensional changes (fuel rod growth)	[ ]	The chromia-doped fuel rod growth correlation will be addressed in a separate topical report.
	vi	Rod internal gas pressure	[ ]	Section 4.6 provides the grain size characterization. Section 7.2 discusses benchmarking the FGR model.

1. Design Bases	Item	Topic	Assessment	Location in this Report
	vii	Assembly liftoff	[ ]	Since neither the method nor calculated results are affected by the use of chromia-doped fuel, this topic is not included in the report.
	viii	Control rod reactivity and insertability	[ ]	Since neither the method nor calculated results for control rod insertability are affected by the use of chromia-doped fuel, this topic is not included in the report. Neutronics methods are discussed in Section 9.3.
B. Fuel Rod Failure	i	Hydriding (fuel rod cladding)	[ ]	Since neither the method nor calculated results are affected by the use of chromia-doped fuel, this topic is not included in the report.
	ii	Cladding collapse	[ ]	Section 4 provides the material properties and Section 9.1 provides analysis results.
	iii	Overheating of cladding	[ ]	Section 4 provides the material properties and Section 9.2 illustrates the impact of chromia-doped fuel on PCT.

1. Design Bases	Item	Topic	Assessment	Location in this Report
	iv	Overheating of fuel pellets	[ ]	Section 4 provides the material properties. Section 9.1 illustrates the impact of the setting of power-dependent LHGR reduction factors for the peak pellet power versus peak pellet exposure-dependent FDL as needed to ensure the AOO licensing criteria are met. Section 9.2 presents the CPR analyses.
	v	Excessive fuel enthalpy	[ ]	Section 5.3.2 discusses chromia-doped fuel behavior during RIA and Section 9.2 illustrates the impact of chromia-doped fuel on deposited enthalpy calculations.
	vi	Pellet/cladding interaction	[ ]	Sections 4 and 7.3 provide the material properties that affect PCMI. Section 9.1 presents the results of the cladding strain analysis. Section 10.2 discusses the ramp test database.

1. Design Bases	Item	Topic	Assessment	Location in this Report
	vii	Bursting	[ ]	Section 9.2 illustrates the impact of Chromia-doped fuel on criteria dealing with swelling and rupture.
	viii	Mechanical fracturing	[ ]	Since neither the method nor calculated results are affected by the use of chromia-doped fuel, this topic is not included in the report.

1. Design Bases	Item	Topic	Assessment	Location in this Report
C. Fuel Cool-ability	i	Cladding embrittlement	[ ]	Section 9.2 illustrates the impact of chromia-doped fuel on criteria dealing with ballooning and rupture.
	ii	Violent expulsion of fuel	[ ]	Since neither the method nor calculated results are affected by the use of chromia-doped fuel, this topic is not included in the report.
	iii	Generalized cladding melting	[ ]	Since neither the method nor calculated results are affected by the use of chromia-doped fuel, this topic is not included in the report.

1. Design Bases	Item	Topic	Assessment	Location in this Report
	iv	Fuel rod ballooning	[ ]	Section 9.2 illustrates the impact of chromia-doped fuel on criteria dealing with ballooning and rupture.
	v	Structural deformation (fuel rod cladding)	[ ]	Since neither the method nor calculated results are affected by the use of chromia-doped fuel, this topic is not included in the report.

4.0 MATERIAL PROPERTIES

Chromia-doped fuel is fabricated by adding a small amount of chromia (Cr_2O_3) [

]. The following sub-sections describe the impact of chromia dopant on the material properties of the chromia-doped fuel in comparison to standard fuel. Throughout the report, the UO_2 fuel is called standard fuel, reference fuel, or non-doped in cases where the contrast to chromia-doped fuel is emphasized.

The chromia-doped fuel manufactured by AREVA is characterized by an additive concentration [ ]. Section 6.0 describes the qualification database which spans the chromia concentration manufacturing uncertainties.

4.1 *Microstructure*

Chromia, Cr_2O_3, is known as an effective dopant to produce fuel with a microstructure characterized by an enhanced grain size, [

]. However, Cr_2O_3 was also found to accelerate fission gas diffusion coefficients when added in quantities of approximately 5000 wppm (Reference 2), which led to dopant segregation on grain boundaries during irradiation. The chromia concentration was established below this concentration level in order to control the dopant distribution within the fuel matrix, while still achieving the goal of having a large grain microstructure.

The fundamental mechanisms governing UO_2 doping with Cr_2O_3 were clarified during the initial development stages in the 1990's. For example, the sintering conditions which favor chromia dissolution in the UO_2 matrix and the solubility limit of chromium in UO_2 were studied. Also, extensive mechanical characterization tests were carried out

on various microstructure types to identify how much Cr_2O_3 is needed to achieve the enhanced viscoplastic behavior for chromia-doped fuel.

The Cr_2O_3-doped UO_2 fuel grain morphology characteristics are specified to achieve the greatest improvement in enhanced fuel viscoplasticity. To that end, the optimum Cr_2O_3 concentration of [ ] was identified, which leads to an average grain size of [ ] as shown in Figure 4-1, and significantly improves the fuel viscoplastic properties.

For the chosen chromia concentration, [

].

4.2 *Theoretical Density*

[

]

The theoretical density of the oxide at 20 °C is equal to the average mass of four molecules composing the elementary cell that is divided by the volume of the elementary cell:

$$\rho_{th} = \frac{4M_{ox}}{N_{av}a_{ox}^3} \quad (4\text{-}1)$$

where:

N_{av} Avogadro's number

a_{ox} oxide lattice parameter

M_{ox} oxide molecular mass

The average molecular weight of the doped oxide is by definition:

$$M_{ox\ doped} = (1 - E_{m\ Cr_2O_3})M_{UO_2} + E_{m\ Cr_2O_3}M_{Cr_2O_3} \quad (4\text{-}2)$$

Finally, the mole fraction of chromia in the oxide, which is needed in Equation 4-2, is given by the following:

$$E_{m\ Cr_2O_3} = \frac{\frac{E_{w\ Cr_2O_3}}{M_{Cr_2O_3}}}{\frac{E_{w\ Cr_2O_3}}{M_{Cr_2O_3}} + \frac{(1-E_{w\ Cr_2O_3})}{M_{UO_2}}} \quad (4\text{-}3)$$

where:

$E_{w\ Cr_2O_3}$ weight fraction of Cr_2O_3 in the oxide

$M_{Cr_2O_3}$ molecular mass of Cr_2O_3

M_{UO_2} molecular mass of UO_2

Therefore, the density of the chromia-doped UO_2 follows from Equation 4-1 by dividing the formulas for doped and standard fuels:

$$\rho_{th\ doped} = \frac{M_{ox\ doped}}{M_{ox}} \quad (4\text{-}4)$$

In formulating Equation 4-4, the experimental finding that the lattice parameter suffers only a minor, negligible decrease was used (Reference 3). Therefore, the parameter $a_{ox\ doped}$ is assumed equal to a_{ox}.

The theoretical density of UO_2 doped with chromia [

], compared to 10.96 g/cm^3 for standard UO_2. A similar small correction is applied to chromia-doped gadolinia fuel.

4.3 *Thermal Expansion*

Thermal expansion of the fuel pellet must be defined in order to calculate heat transfer characteristics of the fuel, which are largely dependent on the gap between the fuel and the cladding. Thermal expansion and pellet swelling due to accumulation of fission gases must be taken into consideration when designing the fuel rod so that adequate clearance is achieved between the cold pellet and cladding during rod loading, and that the pellet-to-cladding gap can be accurately predicted during subsequent irradiation cycles.

When compositional changes to UO_2 may be considered as a solid solution component, these changes have been shown to have a minor influence on the linear coefficient of thermal expansion. This has been demonstrated in the evolution of thermal expansion for mixed oxide (U, Pu) fuel up to 30 wt% PuO_2 addition, and for gadolinia (U, Gd) fuel up to 12 wt% Gd_2O_3 addition. Also, the thermal expansion of irradiated fuel does not significantly differ from unirradiated fuel despite the creation of fission products within the UO_2 matrix as shown in Reference 4.

Therefore, a Cr_2O_3-doping level that is in the range of impurity content has a negligible effect and the thermal expansion of this fuel will be the same as for standard UO_2.

4.4 *Specific Heat and Enthalpy*

Specific Heat (C_p), or specific heat capacity, is an important materials property which is required in order to predict thermal behavior of the UO_2 fuel pellet during the transients considered in reactor safety calculations. Also specific heat is required to compute thermal conductivity from thermal diffusivity, as will be further explained in Section 4.5. The enthalpy and specific heat are coupled, fully correlated variables, with specific heat being the partial derivative of enthalpy with respect to temperature.

The specific heat of unirradiated UO_2 and Cr_2O_3-doped UO_2 fuel pellets was measured by differential scanning calorimetry at the Materials Research Unit of JRC-ITU using a cover gas of high-purity argon and a heating rate of 25 K/min (Reference 15). The relative uncertainty on the specific heat determined by this technique is estimated to be 7% (Reference 15). The JRC-ITU measured values for the specific heat of standard and chromia-doped UO_2 fuel types is displayed in Figure 4-2, in which the high-temperature measurements from previous studies at JRC-ITU (Reference 7) are also shown.

A negligible effect of the chromia additive on the specific heat of UO_2 is observed in Figure 4-2 for the low to medium (about 1500 K) temperature range. The slightly higher specific heat of chromia-doped fuel is in agreement with the law of mixtures and it is appropriate to ignore the negligible increase in specific heat due to chromia additive. The negligible effect of the chromia additive at high temperatures, where data are not available, is justified based on theoretical arguments, which apply over the full temperature domain. The same negligible effect of the chromia additive was also determined for chromia-doped gadolinia fuel.

It is shown in Reference 8 that in the low to medium temperature range the specific heat is well represented by the Debye and Einstein models, which describe the contribution of harmonic and anharmonic lattice vibrations; while at high temperatures (above 1500 K) the rapid increase in specific heat is attributed to point defect formation, especially Frenkel defects (pairs of uranium cation vacancies and interstitials). The chromium additive occupies mostly interstitial positions and has little impact on the uranium cation sub-lattice (although it can affect the oxygen sub-lattice) and thus it does not affect the formation of Frenkel defects at high temperatures. Consequently, the chromium additive has a negligible impact on the Chromia-doped UO_2 specific heat in the high temperature range.

It is concluded that the addition of a small quantity of chromia dopant has a negligible effect on the specific heat of the urania matrix, [ ]. Therefore, chromia-doped fuel will be described with the same specific heat formulation as standard UO_2. Since specific heat and enthalpy are fully correlated variables (the

specific heat is the derivative with respect to temperature of the enthalpy), it can also be concluded that the same enthalpy formulation can be used for chromia-doped fuel as standard UO_2.

4.5 *Thermal Conductivity*

Additives in either substitutional or interstitial solute form cause a decrease in the lattice thermal conductivity because of the additional scattering impact on phonons (quantum particles of the lattice vibration) when the additive has a different atomic mass than the host atoms. Therefore, it was anticipated that chromia doping (atomic mass 52 for chromium compared to 238 for uranium) will decrease the UO_2 thermal conductivity, as was also experienced with other doped fuel types, such as gadolinia fuel.

In order to quantify the chromia doping impact on UO_2 thermal conductivity, diffusivity measurements were performed on chromia-doped UO_2 and gadolinia fuels, as well as standard UO_2, using the laser flash technique.

4.5.1 Laser flash diffusivity technique

To perform laser flash diffusivity measurements, a thin disc specimen is subjected to a radiant energy pulse with high-intensity and short duration. The energy of the pulse is absorbed on the front surface of the specimen, and the resulting rear face temperature rise as a function of time is recorded (Figure 4-3). The thermal diffusivity value is then calculated as a function of the specimen thickness and the time required for the rear face temperature rise to reach certain percentages of its maximum value (References 5 and 6).

The samples are heated to the desired temperature in a tube furnace, or heated with simultaneous high power pulses as in the JRC-ITU very high temperature technique (Reference 7 and Figure 4-4). Measurements are typically performed at several temperature levels, with long enough hold times at each temperature in order to achieve stable conditions before performing the measurement. The maximum achievable temperature level is limited by the furnace, being approximately 1650°C for the measurements reported herein. The temperature is measured directly on the sample by

a certified W (tungsten) thermocouple. Most experiments were conducted under inert gas atmosphere (argon).

The thermal conductivity is not directly measured by this laser flash technique, which is a dynamic type thermal property measurement of thermal diffusivity. Instead the thermal conductivity is calculated as a function of diffusivity, density, and specific heat as shown in Equation 4-5.

$$k(T) = \alpha(T).\rho(T).c_p(T) \quad (4\text{-}5)$$

where:

k(T)	-	thermal conducitvity	[W/mK]
α(T)	-	diffusivity	[m^2/s]
ρ(T)	-	density	[kg/m^3]
c_p(T)	-	specific heat	[J/kg]
T	-	temperature	[K]

In most cases reported in the literature, specific formulations have been used for the density and specific heat. Moreover, for some JRC-ITU data, the actual measured specific heat values have been used. In order to eliminate this additional source of scatter, all the diffusivity data employed in this report have been processed with the specific heat formulation recommended by the MATPRO compendium of nuclear materials properties (Section 2.2 of Reference 8).

4.5.2 Chromia-doped thermal diffusivity database

Two in-house laser flash diffusivity measurement campaigns were conducted in 2006 and 2015. In addition, in both cases a sub-set of samples used for the in-house measurements were sent to JRC-ITU for complementary measurements.

[

]

Figure 4-5, Figure 4-6, Figure 4-7, and Figure 4-8 display the results (all conductivity values normalized to 95% TD) of the two measurement campaigns both in-house and at JRC-ITU. The following general observations can be drawn from the two measurement campaigns:

[

]

[

]

4.6 *Grain Size and Growth*

The enlarged grain microstructure is one of the two major features of the chromia-doped fuel that are different from the standard UO_2 fuel, the other one being the thermal conductivity. There have been a number of chromia-doped lots fabricated in small scale batches for the different lead fuel assembly (LFA) programs and one large-scale study, with the reported grain sizes listed in the first column of Table 4-3.

Grain growth occurs by grain boundary migration so that the larger grains are enlarged at the expense of the smaller adjacent grains. Therefore, it is expected that very little grain growth occurs in the chromia-doped fuel during irradiation since considerable grain growth already occurred during sintering. This leads to a stable grain structure.

[

]

4.7 *Elastic Moduli*

The possible variation of elastic properties is not fundamentally affecting the fuel behavior under normal operating conditions or AOO and accidental conditions.

According to the data published in the literature, the Young's modulus of standard UO_2 can vary with characteristics such as grain size, stoichiometry or fuel porosity, however, the effect of these parameters is very limited compared to that of temperature (Reference 9). Moreover, the intrinsic impact of additives, including gadolinium or plutonium, up to high amounts (10-20 wt%) remains low with respect to Young's modulus and negligible for Poisson's ratio (Reference 9).

Considering that the chromia addition in UO_2 is low [ ], no effect is anticipated on the UO_2 fuel Young's modulus and Poisson's ratio. Therefore, the same models that are currently used for standard fuel remain applicable to chromia-doped fuel.

4.8 *Tensile Fracture Strength*

During normal steady-state or variable power conditions, the fuel pellet develops cracks because the thermal stresses, which are created by the quasi-parabolic temperature distribution across the fuel pellet, reach values above the fracture strength of the fuel.

Consequently, the fuel fracture strength is important. As a general trend, UO_2 tensile strength decreases when the deformation rate increases, and this trend is more pronounced at high temperature. At room temperature, UO_2 tensile strength decreases with increases in fuel pellet porosity, pore size and grain size.

The transition temperature between brittle and ductile behavior increases with increased grain size and the fuel tensile strength is reduced by approximately 40% (Reference 10). Finally, the effect of additives on fuel fracture strength is the result of microstructural modifications induced in the fuel matrix.

Comparative studies between UO_2 and Cr_2O_3-doped unirradiated fuels were performed by AREVA [

]

This behavior for the chromia-doped fuel is fully consistent with results published in the literature (Reference 11) and accounts for the Chromia-doped fuel matrix with larger grain size. The plasticity temperature is lowered and therefore the bridging annulus is closer to pellet outer radius, meaning a narrower cracked outer rim with more numerous and smaller radial cracks, which is beneficial for PCI performance.

4.9 *Creep and Plastic Deformation*

For standard UO_2 fuel (unirradiated samples), significant steady-state thermal creep occurs for temperatures exceeding approximately 1100 °C. Two creep mechanisms are active depending on the magnitude of the applied stress in comparison to a transition stress (σ_t) (dependent on the matrix grain size) as follows:

- $\sigma < \sigma_t$: pellet deformation according to diffusion creep mechanisms and inversely proportional to the matrix grain size
- $\sigma > \sigma_t$: pellet deformation according to dislocation creep mechanisms and independent of the matrix grain size

The effect of additives on fuel steady-state creep behavior is difficult to identify because it is compounded with other fuel matrix characteristics affected by the additive: grain size, stoichiometry, equilibrium defect concentration, formation of secondary phases -- all things which might change diffusion coefficients, and/or grain boundary properties.

To assess the viscoplastic properties of the chromia-doped UO_2 fuel pellets, extensive uniaxial mechanical compression tests were performed. These tests were performed under controlled atmosphere to prevent oxidation and stoichiometry changes of samples during the measurements. The main findings for the Cr_2O_3-doped fuel are summarized below.

[

]

Contrary to standard fuel with a smaller grain size, the viscoplastic deformation of the doped fuel [

].

4.10 *Fuel Pellet Cracking*

An adequate description of the crack patterns (number of cracks and orientation) which develop in fuel pellets during base load operation (including power ramps) is needed in order to calculate fuel pellet deformation and hence the pellet-clad mechanical interaction.

As the fuel rod power increases, pellets crack due to thermal stresses induced by the radial temperature gradient. At beginning of life, the minimum power required to initiate this radial cracking is approximately [ ]. However, while certain crack patterns are always noted after irradiation, there are no direct observations of the crack patterns at power. Inferences must be made on the basis of the parameters that are known to be important: the irradiation conditions, the fuel rod dimensions, and the cladding properties.

As discussed in Section 4.8, chromia doping affects the pellet tensile fracture strength and therefore also affects the fuel cracking pattern in operation. However, from the comparison given in Figure 4-13, it appears that Cr_2O_3-doped fuel cracking is fundamentally the same as for UO_2. In both cases, the main cracking component is radial, due to the tensile tangential stress in the outer pellet annulus. The circumferential crack is assumed to be formed, as generally accepted, during cooling at the final shut down.

It was observed from hot-cell PIE of chromia-doped fuel pellets following steady-state irradiations that a similar number of radial and axial cracks are present for both PWR and BWR fuel rods. After power ramp testing, it was observed that in comparison to standard fuel, [

].

4.11 *In-reactor Densification*

In-reactor densification is a phenomenon induced by irradiation and is thermally activated. Densification results from the elimination of fine porosity. First, the small-sized porosities (less than 1 μm) disappear, and then the medium-sized pores (about 1 to 3 μm) are progressively eliminated. The densification phase results in an increase of the fuel density by a decrease in the volume. The kinetics and the magnitude of the densification depend mainly on the fuel porosity distribution, which is a function of the powder used and of the pellet production process.

For such oxide fuels, experimental results have shown that the density variation observed under irradiation was close to that observed after a 24-hour out-of-reactor thermal stability test at 1700 °C, even if the mechanisms involved are different. Therefore, the resintering data are used to quantify the in-reactor densification of any fuel types.

[

]

4.12 *Effect of Additive on the High Burn-up Fuel Pellet Rim Structure*

A local burnup of about 60 MWd/kgU at the pellet periphery is usually considered necessary for initiation of the high burnup structure (HBS) in UO_2 fuel under low temperature conditions of less than 500 °C (Reference 12). [

]

This behavior is consistent with previous studies such as those reported in Reference 13. Grain recrystallization can develop when nucleus grains, i.e. sub-divided grains, are present. It is hypothesized that nucleus grains with high-angle grain boundaries are formed by inhomogeneous accumulations of dislocations.

In particular, grain boundaries are special areas for inhomogeneous dislocation accumulations because they inhibit the motion of dislocations. A smaller grain size will have a larger grain boundary surface area per volume, which will result in a higher density of dislocations. Such a fuel matrix will be prone to recrystallization, in contrast to a large grain matrix. [

]

The main conclusions from AREVA hot-cell PIE studies regarding HBS of chromia-doped fuel are as follows:

[

]

Overall, there is no significant difference in burnup thresholds and porosity of the HBS compared to standard fuel. The following trends were observed:

[

]

Table 4-1 Thermal Conductivity Test Database Composition, 2015

[

]

Table 4-2 Thermal Conductivity Test Database, 2015 – Material Characteristics

[

]

Table 4-3 Grain Sizes of Chromia-Doped Database

[

]

[

]

Figure 4-1 Illustration of Grain Morphology in Standard and Chromia-Doped Fuels

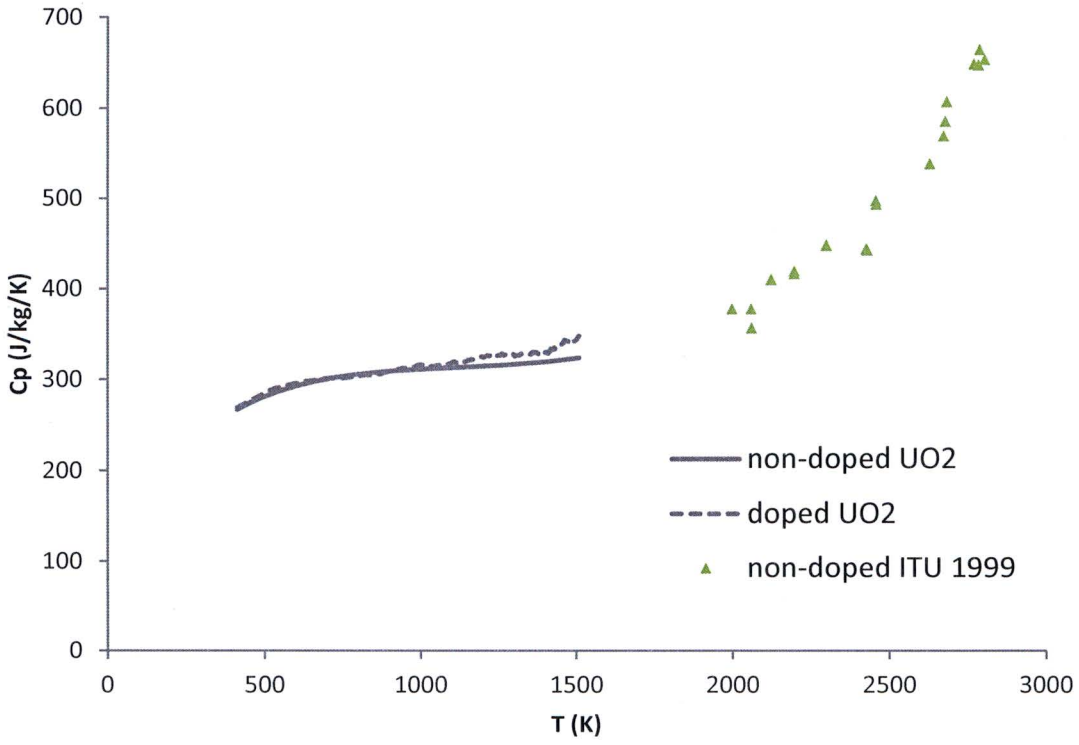

Figure 4-2 Specific Heat Measurement Data at JRC-ITU of Doped and Non-Doped Fuels

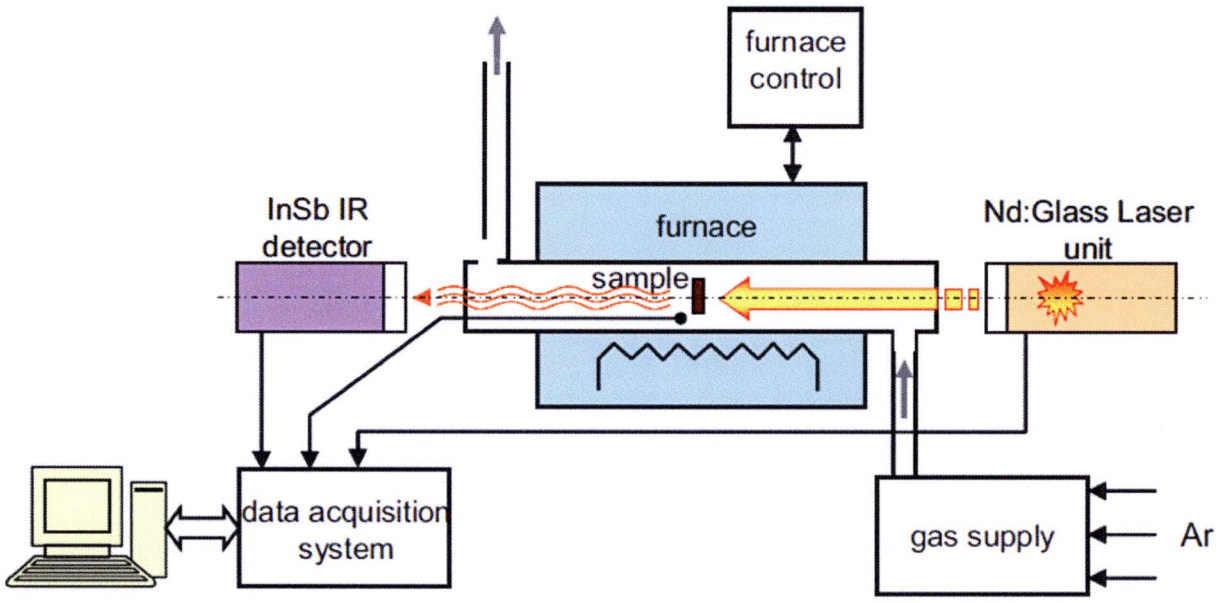

Figure 4-3 Experimental Laser-flash Technique to Measure Thermal Diffusivity at Low to Medium Temperatures

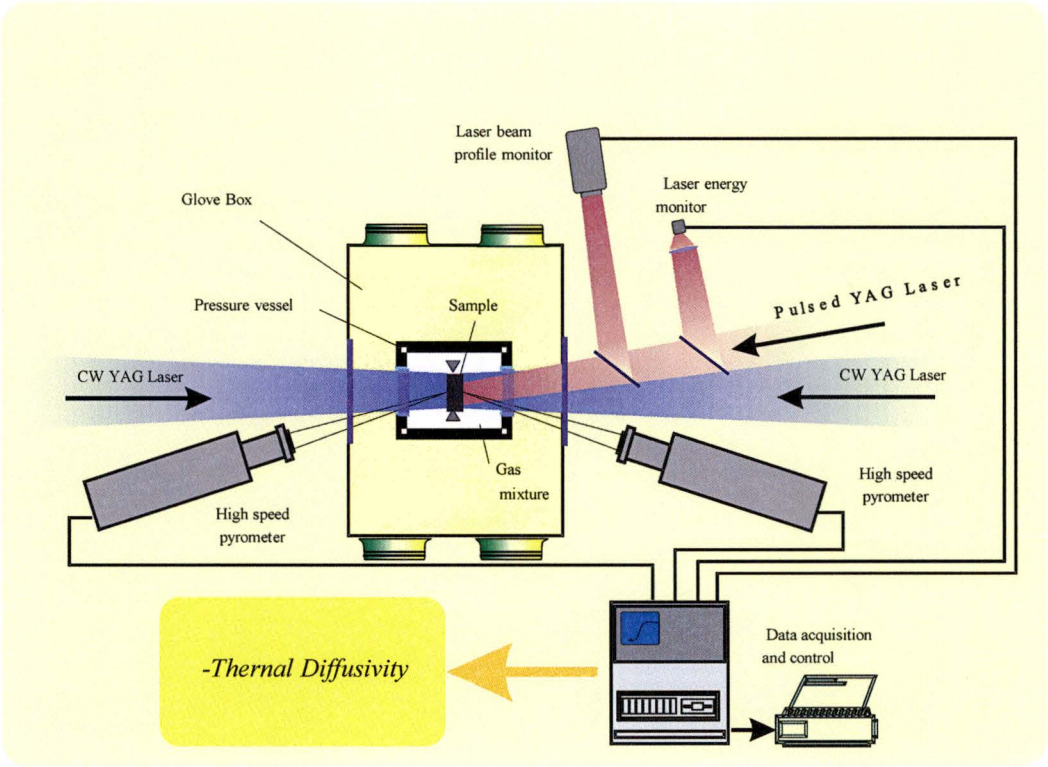

Figure 4-4 Schematic Diagram of Laser Flash Thermal Diffusivity Apparatus for High Temperature used at JRC-ITU

[

]

Figure 4-5 Thermal Conductivity Measurements at AREVA in 2015

[

]

Figure 4-6 Thermal Conductivity Measurements at JRC-ITU in 2015

[

]

Figure 4-7 Thermal Conductivity Measurements at AREVA in 2006

[

]

Figure 4-8 Thermal Conductivity Measurements at JRC-ITU in 2006

[

]

Figure 4-9 Diffusivity Measurements at JRC-ITU on AREVA Doped and Non-Doped Fuels

[

]

Figure 4-10 Yield Strength of Doped and Non-Doped Fuels at 1500℃

[

]

Figure 4-11 Creep Strain of Doped and Non-Doped Fuels at 1500℃

[

]

Figure 4-12 Comparison of Creep Data for Doped and Non-Doped Fuels

[

]

Figure 4-13 Post-Irradiation Ceramography Comparing Doped and Non-Doped Fuels

5.0 BEHAVIORAL ASSESSMENT

The chromia-doped fuel behavior described in this section refers to special cases of either fuel failure or accident situations; and fuel melting is therefore included here as it is a key parameter for AOO and accidental conditions.

The behavior during accident conditions is analyzed with safety codes and methods. The adaptation of the codes and methods for application to chromia-doped fuel is described in Section 8.0 with sample problems provided in Section 9.0.

5.1 *Washout Characteristics*

Failed fuel degradation after the occurrence of primary defects (fuel rod leaks) can significantly affect reactor operations. As occasionally observed during some BWR fuel failures, axial split-type secondary failure of cladding results in a large release of fission products into the reactor coolant and may also lead to fuel washout due to direct contact of the fuel pellets with the coolant. Even though there are no licensing methodologies or criteria associated with washout, out-of-pile lab testing was performed to assess the washout behavior of chromia-doped pellets for comparison to standard UO_2 fuel.

First, the reaction of fuel pellets with oxygen has been investigated by thermogravimetry at 380 °C (Reference 33). For a better understanding of the mechanisms involved, various types of Cr_2O_3-doped pellets having different density and grain size characteristics were tested (Table 5-1). The absolute mass changes that were measured during the tests showed that samples A and B, corresponding to the optimum grain size chromia-doped fuel, has up to 50% improved resistance against oxidation; while the chromia-doped sample C with a smaller grain size shows roughly a similar behavior to standard UO_2.

In Figure 5-1, ceramographic examinations show the difference in the oxidation occurring in the different fuel pellet samples. For standard UO_2, an intergranular corrosive attack is revealed with an outer surface oxidation which is quickly followed by intergranular oxidation and cracking and later spalling of oxidized grains. Similar features also appear in the case of the chromia-doped sample C.

On the contrary, in the case of the optimum grain size chromia-doped fuel samples A and B, the oxidation of the outer surface is not accompanied by generalized oxidation along grain boundaries. The outer oxidized layers are a barrier for oxygen diffusion and therefore the oxidation rate diminishes in time with very few intergranular cracks being formed. Thus, the larger grain size characteristic of chromia-doped fuel is the key parameter for reducing fuel oxidation.

In a second study, fuel corrosion behavior was investigated in autoclave leaching tests performed under representative BWR conditions (360 °C – 70 bars – 70 ppm H_2O_2 in feed water), which showed [

]. Examinations of chromia-doped samples from this second study showed:

[

]

The oxidation and washout behavior of unirradiated standard and Cr_2O_3-doped UO_2 fuel pellets have been analyzed in the two studies described above by thermogravimetry and by autoclave leaching tests at BWR conditions, respectively. The testing program demonstrates that chromia doping enhances the corrosion resistance of the fuel pellets. Such a feature is desired to prevent fuel pellet disintegration in case of failed fuel rods and the resulting contamination of the LWR primary coolant.

The main driver of the corrosion resistance improvement is [

].

It is worth noting that this trend observed in unirradiated fuel samples remains valid for irradiated fuel. This is supported by the conclusions drawn from the studies reported in Reference 14. More particularly these studies highlighted that the grain boundary penetration corrosion depths of irradiated pellets are approximately equivalent to values for unirradiated pellets. Consequently, it was stated that fuel irradiation, i.e. accumulation of fission products and irradiation damage, had no significant effect on the fuel corrosion.

5.2 *Fuel Melting*

One of the variables that influence the melting point of UO_2 is the total quantity of elemental impurities dispersed within the crystal structure. As impurities or trace dopants increase in UO_2, the melting point decreases.

The impact of chromia dopant on the melting temperature was determined by measurements performed at JRC-ITU (Reference 15) on standard and doped uranium dioxide, as well as chromia-doped (U-Gd) O_2 samples.

The melting temperature was determined by laser heating and fast multi-channel pyrometry, an experimental method developed at JRC-ITU (References 16 and 17). The technique is illustrated in Figure 5-3. During the laser heating, a mixed oxide disk is held in a sealed autoclave under a controlled atmosphere (slightly pressurized air or argon at 0.35 MPa). In experiments carried out in pressurized argon, the absolute pressure of oxygen was checked to be smaller than 10 Pa. The controlled atmosphere together with the relative short duration of the experiments permitted only minimal sample decomposition, particularly linked to oxidation or oxygen losses, depending on

the initial composition. This approach aims to maintain the sample integrity and its composition as close as possible to its initial nominal value throughout the melting and freezing process.

Thermograms were measured with sub-millisecond resolution pyrometry on samples laser heated beyond melting. Pulses of different duration (100 ms to 1000 ms) and maximal power (315 W to 585 W) were repeated on a 5 mm diameter spot on a single sample surface, as well as on different samples of the same composition in order to obtain statistically significant datasets for each composition. Such pulses lead to maximum temperatures between 3500 K and 4000 K, which are considerably higher than the known melting temperature of uranium dioxide. This allows a sufficient amount of material to melt during the test in order to obtain a consistent thermal analysis during the cooling stage of the experiment.

Excessive thermal shocks were minimized by starting each series of laser pulses from a pre-set temperature of about 1500 K, at which each sample was held for 30 seconds before starting a series of high-power laser pulses. The pre-heating treatment also ensured better homogenization of the sample surface.

Each series consisted of four heating-cooling pulses on the same sample spot without cooling the material below an intermediate temperature of approximately 1500 K. The peak intensity and duration of the high power pulses were changed from one heating-cooling cycle to the other, in order to check the repeatability under slightly different experimental conditions and the effect of non-congruent vaporization or segregation phenomena. The sample cooled naturally when the laser beam was switched off during the thermal cycle. Thermal arrests corresponding to exothermic phase transitions (solidification) were then observed on the thermograms recorded by the fast pyrometers. The results are listed in Table 5-2 and Table 5-3 for chromia-doped UO_2 and chromia-doped gadolinia fuels, respectively.

The test data was processed to determine the melting point of chromia-doped fuel on the following basis:

[

]

Applying this methodology to the data presented in Table 5-2, the fuel melting temperature of chromia-doped UO_2 is [ ] in comparison to standard UO_2 fuel.

With respect to gadolinia fuel, [

] This conclusion is validated by the measurements performed at JRC-ITU (Table 5-3) which show that [

].

5.3 *Behavior During Accidental Conditions*

The following two sections justify the conclusion that the anticipated behavior of chromia-doped fuel during the LOCA and RIA design basis accidents is [

].

5.3.1 Loss of coolant accidents

During normal operation, oxide fuel pellets develop many radial and transverse cracks because of the thermal stresses generated by the quasi-parabolic radial temperature distribution across the fuel pellet. Therefore, the pellet can be viewed as a conglomerate of several millimeter-sized cracked fragments that are only loosely joined. During a temperature transient associated with a LOCA scenario, the cladding can deform outward due to loss of primary system pressurization (the term ballooning is

used for this process). It is possible that some of the fragments may move out of place and fill the additional open void created by the ballooning.

At high burnup however, several new phenomena are encountered which may counteract this behavior during a LOCA event. With the onset of pellet-to-cladding contact, bonding develops between the fuel pellet and the cladding. The higher the burnup, the thicker and larger the circumferential and axial surface coverage of the bond layer becomes. The development of this bond layer inhibits the ability of the pellet and cladding to move independently, and thereby affects load transfer from the pellet to the cladding and the subsequent cladding stress state. Another high burnup effect is the increasing amount of fission gas atoms in the fuel which may result in gaseous bubble swelling of the fuel when it reaches high temperatures. A third high burnup effect that might have an impact on LOCA behavior is related to the high burnup structure (HBS) at the pellet rim, with its associated large pores.

The LOCA testing programs at Studsvik and Halden have identified a tendency towards fine fuel fragmentation (called pulverization) and dispersal for simulated LOCA tests on high burnup fuels. It was identified that the susceptibility to pulverization is highly correlated to the formation of HBS at the rim of the pellet (Reference 18).

With respect to all these phenomena, chromia-doped fuel behaves [

]

5.3.2 Reactivity initiated accidents

A Reactivity-Initiated Accident (RIA) is a nuclear reactor accident that involves an unwanted increase in fission rate and reactor power. The immediate consequence of a

RIA is a fast rise of fuel power and temperature. The power excursion may lead to failure of the nuclear fuel rods and release of radioactive material in the primary reactor coolant.

Pulse irradiation tests show that fuel rod susceptibility to failure increases with increasing fuel burnup. It is also clear that the burnup dependent state of the rod and, in particular, the degree of waterside corrosion and related hydride induced embrittlement is very important for the survivability of fuel rods. Regarding fuel pellets, the factors of particular importance to the behavior include: heat-up rates, melting, fragmentation, fission gas induced transient swelling and transient fission gas release.

Under the initial phase of a RIA, the fuel pellet is heated almost adiabatically, i.e. without heat transfer taking place either inside the fuel pellets or across the pellet-clad gap. Due to the surface-peaked temperature distribution in combination with the burnup-induced depression of fuel melting temperature at the pellet periphery, peak temperature under rapid RIAs will first occur at a radial position of about 0.2 to 0.5 mm beneath the pellet surface. To extend the discussion on fuel temperature and the potential risk for fuel melting with a change from UO_2 to chromia-doped fuel it is necessary to consider that:

[

]

All these elements indicate that the radial average fuel enthalpy threshold for incipient melting of chromia-doped fuel is not significantly different from the UO_2 fuel enthalpy threshold.

In ceramography examinations of high burnup fuel which has undergone a simulated RIA in pulse reactors, it is usually found that the outermost part of the pellet is fragmented. Typically a large number of radial cracks are seen at the pellet surface, and these cracks extend a few millimeters towards the fuel center, i.e. well beyond the re-structured rim zone.

These cracks are attributed to the large tensile radial and hoop stresses created during the early heat-up phase. The cracked fragments are large in size for low to medium burnup fuel, but for high burnup fuel, much finer fragments (less than 50 μm) have been observed in post-test examinations. These small-size fragments are found predominantly in the external part of the UO_2 fuel pellets and are potentially available for fuel dispersal after fuel rod fracture during a severe RIA transient. The fine fragments are most likely a result of grain boundary decohesion, caused by over-pressurization of gas filled pores and intergranular bubbles under rapid rise in temperature (Reference 19).

[

]

Table 5-1 Fuel Sample Characteristics for Thermogravimetry Testing

Pellet type	Pellet density (% TD)	Pellet grain size (μm)	
		Linear intercept value	3D calculation value
Standard UO_2	97.0	8	12
Cr_2O_3-doped – A	97.1	57	89
Cr_2O_3-doped – B	98.2	55	86
Cr_2O_3-doped – C	96.8	28	44

Table 5-2 Melting Temperature Measurements of Doped and Non-Doped samples at JRC-ITU

[

]

Table 5-3 Melting Temperature Measurements of Doped and Non-Doped Gadolinia Fuel Samples at JRC-ITU

[

]

[

]

Figure 5-1 Fuel Ceramography Showing Reduced Oxidation of Doped Fuel in Comparison to Non-Doped Fuel

[

]

Figure 5-2 Grain Structure Showing Reduced Oxidation Penetration of Doped Fuel

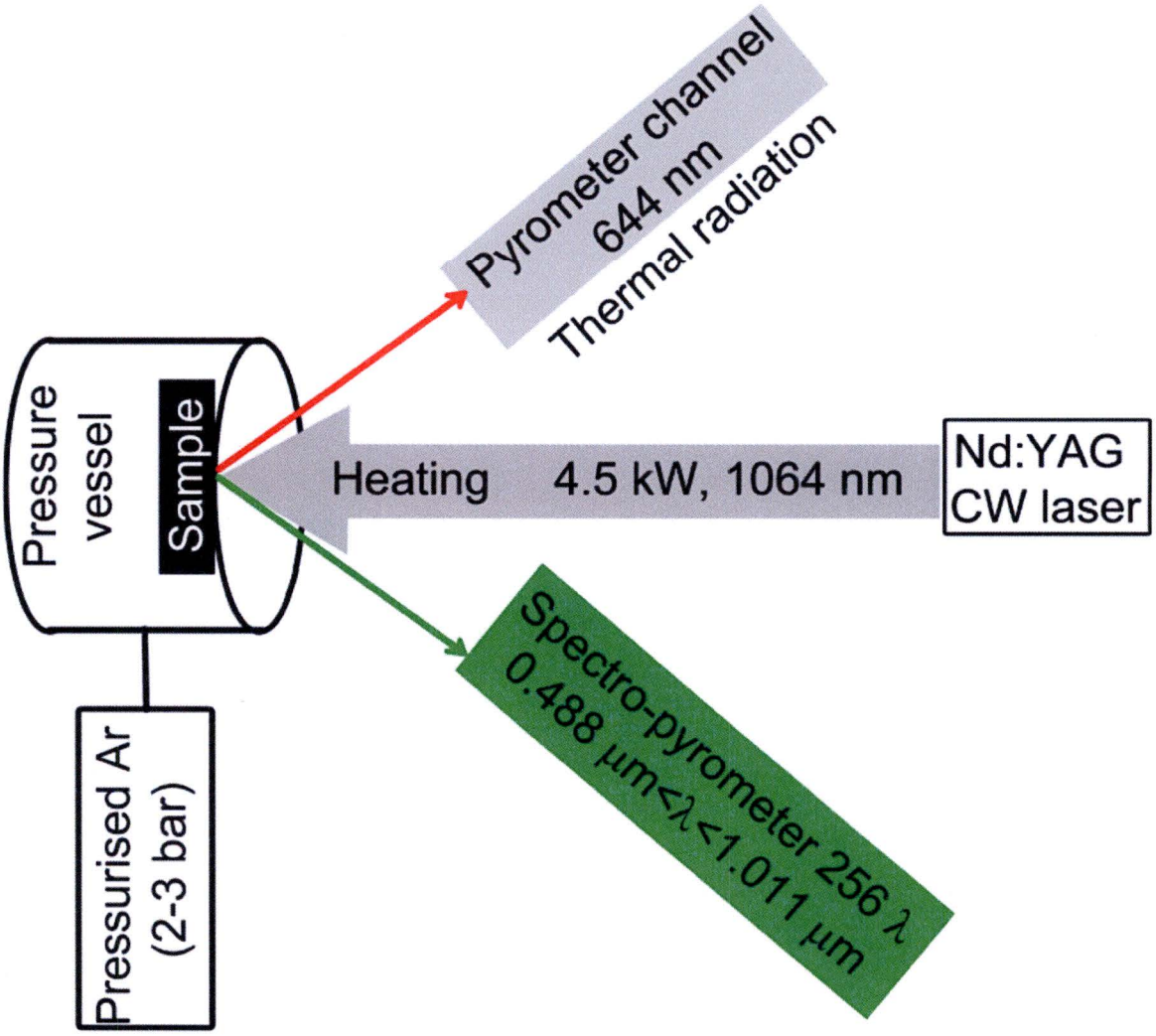

Figure 5-3 Melting Temperature Experimental Setup at JRC-ITU

6.0 QUALIFICATION DATA

The program to develop and study chromia-doped fuel pellets was initiated almost twenty years ago in French PWRs with actual plant irradiations starting in 2001. The irradiation program continued with operation in base load and load-follow transient conditions up to 75 MWd/kgU.

A large set of irradiation data in both power reactors and research reactors in steady-state and power ramp operational modes and in conditions specific to both BWR and PWR reactors was acquired in the last fifteen years. This comprehensive database covers the application range in terms of burnup and power, and is used to qualify the fuel codes for application to chromia-doped fuel. [

]

6.1 *Steady-state Qualification Dataset*

The chromia-doped fuel was irradiated in both BWR and PWR fuel rods, covering a range of designs and cladding materials. The range of the burnup achieved during steady-state irradiations is summarized in Table 6-1.

The cladding materials for the chromia-doped steady-state database are as follows:

[

]

The following fuel rod designs were used for the chromia-doped steady-state database:

[

]

Following irradiation, the following PIE measurements were acquired:

[

]

The fuel rods were either full-length or a string of rodlets that underwent power ramps in research reactors after the base irradiation. In some irradiation campaigns, rods with standard fuel were also irradiated in the same fuel assembly as the rods with chromia-doped fuel.

[

]

Temperature measurements were collected to support separate effects testing for high burnup fuel (~60 MWd/kgU). A segment cut from a rod base-irradiated in a commercial reactor was refabricated and instrumented with a central thermocouple and further irradiated in a test reactor with on-line temperature measurement during the steady state phase and two intermediate steps to higher power levels.

[

]

6.2 *Ramp Database Qualification Dataset*

The cladding materials for the chromia-doped power ramp database are as follows:

[

]

The following fuel rod designs were used for the chromia-doped steady-state database:

[

]

Following irradiation, in which the burnup range is summarized in Table 6-1, the following PIE measurements were acquired:

[

]

The power ramp parameters, conditioning power level, power increment and hold time at the ramp terminal power level which were achieved in both the BWR and PWR power ramps programs cover the operational domain. This ramp test data has been used to determine the PCI benefit of the chromia-doped fuel as decribed in Section 10.2.

[

]

[

]

* ATRIUM is a trademark of AREVA Inc.

Table 6-1 Chromia-Doped Fuel Irradiation Database

[

]

7.0 QUALIFICATION OF RODEX4 FOR CHROMIA-DOPED FUEL

The RODEX4 fuel code was approved for BWR fuel rod design and licensing analyses in conjunction with its associated realistic methodology (Reference 20). The unique properties of chromia-doped fuel, which have been described in Section 4, necessitate minor adaptation of select code models so that RODEX4 can be applied to chromia-doped fuel for BWR analyses using the same realistic methodology.

The verification and validation of RODEX4 for qualification to chromia-doped fuel used the qualification database presented in Section 6 and consists of the following:

[

]

The qualification of RODEX4 to chromia-doped fuel also justifies the removal of the grain size restriction imposed in the Safety Evaluation for Reference 20. The qualification database includes larger grain sizes as indicated in Table 4-3.

The following describes the model adaptations or additions that were required, as well as the benchmarking of the qualification database. [

]

7.1 *RODEX4 Thermal Conductivity Model for Chromia-doped Fuel*

The JRC-ITU 1999 data (Reference 7) are generally considered the most qualified laser flash diffusivity data and therefore are used to validate the RODEX4 thermal conductivity model. As stated in Section 4.5, the 1999 JRC-ITU thermal conductivity

values were calculated by using either JRC-ITU measured specific heat or a known correlation for the specific heat. Therefore the calculation versus measurement comparison of thermal conductivity is significantly affected by which specific heat correlation was used to derive thermal conductivity from the measured thermal diffusivity.

The specific heat model in RODEX4 was taken from the MATPRO library of material properties prepared by INL (Reference 8), which is widely used in the nuclear industry. Another common source for specific heat is the material properties compendium sponsored by IAEA (Reference 21) largely based on the work led by J.K. Fink at ANL (Reference 22). The two specific heat correlations are quite comparable, with about 1% relative difference in the low to medium temperature range and larger differences of up to 4% relative in the high temperature range, as can be observed in Figure 7-1.

The JRC-ITU 1999 thermal conductivity values reported in Reference 7 used the Fink specific heat formulation for the low temperature range and their own measurements for the high temperature range. RODEX4 (i.e. MATPRO) over-predicts those data, especially in the high temperature range where the measurements present a large scatter band. The directly measured quantity is thermal diffusivity, while the thermal conductivity is calculated using a specific heat correlation that is independently obtained from separate measurements. To have an equivalent comparison of thermal conductivity, it is necessary to recalculate thermal conductivity from the thermal diffusivity data in Reference 7 using a common specific heat correlation.

The effect of using the specific heat correlation and density relations from RODEX4 (taken from MATPRO) to convert the JRC-ITU 1999 thermal diffusivity data into thermal conductivity is illustrated in Figure 7-2. This figure shows that the re-evaluation of thermal conductivity leads to a better agreement with the RODEX4 model. Therefore, it is concluded that the JRC-ITU 1999 laser flash measurements are in reasonable agreement with the RODEX4 model when a consistent specific heat correlation is used.

It is noticeable that the high temperature scatter band for thermal conductivity is greatly reduced when using the MATPRO specific heat formulation, which results from

elimination of the large uncertainty range of the JRC-ITU specific heat measurements in this high temperature range.

The results of the previous analysis have been further confirmed by including the JRC-ITU measurements of standard UO_2 from the two campaigns conducted by AREVA on chromia-doped fuel (see Section 4.5). In order to remove inconsistencies related to the specific heat formulation used, the thermal diffusivity was calculated with the RODEX4 model and compared to measured thermal diffusivity values, corrected to 95% theoretical density. The results demonstrate a best-estimate prediction over the whole temperature range (Figure 7-3). It is observed that AREVA data from the two chromia-doped campaigns fill most of the gap in the temperature domain that was not covered by the JRC-ITU 1999 data and demonstrate consistency among the three datasets and with the nominal RODEX4 model.

The adaptation of the RODEX4 thermal conductivity model and its subsequent validation is discussed below.

7.1.1 Adaptation of RODEX4 thermal conductivity model to unirradiated chromia-doped fuel

The processing of the chromia-doped measurements described in Section 4.5 started with the linear fit of the inverse conductivity (thermal resistivity) after normalizing the raw data to 95% theoretical density according to the porosity term in RODEX4. A linear fit is expected for the low temperature range where the phononic term (Equation 7-2) dominates. The anticipated effect of chromia additions was confirmed by this linear plot of the inverse of conductivity, as displayed in Figure 7-4. The thermal resistivity increases (and thermal conductivity decreases) as the chromia content increases.

The dopant effect on thermal conductivity is the result of scattering phonon interactions (lattice vibrations) with impurities in the lattice either in substitutional or interstitial form. The impurities increase the thermal resistance of the lattice to phonon transport and therefore decrease the phonon conduction. The intrinsic thermal resistivity of the lattice is caused by phonon-phonon scattering interactions which increase in strength with temperature. [ ]

[

]

[

]

For completeness, the final adjusted model parameters of the chromia-doped thermal conductivity are listed below in Equations 7-1 to 7-9 and displayed in Figure 7-5:

[

]

[

]

7.1.2 Validation of RODEX4 thermal conductivity model to irradiated chromia-doped fuel

The previous thermal conductivity model adaptation to chromia-doped fuel was based on unirradiated fuel studies and accounts for the generic impact of the chromia dopant. It was anticipated that the burnup degradation impact on thermal conductivity, as described by Equation 7-5 for standard fuel, is valid for chromia-doped fuel as it was previously shown to be valid in the case of gadolinia fuel.

This was confirmed by the benchmarking of the REMORA2 test in which the pellet centerline temperature was measured online by a central thermocouple that was inserted in the drilled section of the refabricated rodlet. The rodlet was irradiated in the SILOE test reactor after the father rod achieved a rod average burnup of ~ 62 MWd/kgU in a power reactor.

Figure 7-6 below compares calculated and measured temperatures of the REMORA2 tests and demonstrates good agreement over the whole range of test powers. This is further illustrated in Figure 7-7, which shows the same trend vs power for both calculated and measured temperatures. A slight over prediction at the high power end is well within the power uncertainty range.

7.2 *RODEX4 Fission Gas Release Model for Chromia-doped Fuel*

Chromia-doped fuel is similar to standard fuel with an enlarged grain microstructure and the same phenomenological FGR model is applicable to both fuel types. In addition, the more oxidizing sintering conditions and the presence of the aliovalent chromia-dopant lead to a special electrochemical state of the chromia-doped fuel that is prone to enhancing diffusion processes which promote enhanced creep and grain growth during sintering. Hence a certain augmentation of the gas atom diffusion was speculated as possible for chromia-doped fuel. [

]

Therefore, the FGR model was not changed for chromia-doped fuel. It is remarked that the larger grain microstructure has two main consequences with opposite effects on FGR. On one hand, the gas atom diffusion to grain boundaries is delayed and diminished, but on the other hand, the grain boundary area and hence the grain boundary gas atom saturation (retention) capacity is decreased. While the first effect leads to FGR reduction, the latter causes a FGR increase. The net result is therefore time and power history dependent. The benchmarking of the chromia-doped FGR database was assessed in conjunction with the standard rods that were irradiated in the same fuel assemblies with the chromia-doped fuel rods, and for which FGR measurement was available.

The larger grain size of the chromia-doped fuel delays the transport of gas atoms to the grain boundary and therefore delays and reduces the final fission gas release to open voidage. Therefore, an exact and proper definition and characterization of the grain size of chromia-doped fuel is crucial for an adequate calculation of FGR. The existing

database consists of chromia-doped fuel manufactured in a small trial and production size setting, with variations and differences in powder mixing and sintering conditions.

[

]

The calculation versus measurement comparison is displayed Figure 7-8. [

]

7.3 *RODEX4 Intragranular Gaseous Swelling Model for Chromia-doped Fuel*

The PIE data on chromia-doped fuel rods show larger cladding deformation following both steady-state and power ramp irradiations, which indicates an increased chromia-doped fuel pellet deformation in comparison to standard fuel. Ceramography data show that larger intragranular bubbles exist in the case of chromia-doped fuel, which corroborates with the observed larger cladding deformation. These larger bubbles are interpreted to be a consequence of enhanced intragranular gaseous swelling, which in turn contributes to larger pellet deformation and hence larger cladding deformation, especially during power ramps. Standard UO_2 exhibits very low intragranular gaseous swelling so this has not been modeled previously in RODEX4. The difference in intragranular gaseous swelling can be observed in hot-cell PIE images (Figure 7-9) indicating a low gas precipitation on grain boundaries and a significant gas precipitation into intragranular bubble form.

The larger intragranular gaseous swelling of the chromia-doped fuel is due to the combination of the two main characteristics of this fuel type: larger grain size and enhanced creep and plasticity. The latter implies greater propensity of the bubbles inside the grain to grow to larger size. The larger grain size means a greater chance for gas atoms being trapped by bubbles as they diffuse towards grain boundaries.

Consequently, an intragranular gaseous swelling model was developed for chromia-doped fuel in RODEX4. [

]

The hot-cell PIE performed by CEA for AREVA was used to determine the expected range for the model parameters defined above, the most important features revealed by PIE (see Figure 7-9) in relation to intragranular swelling being as follows:

[

]

Then, the number of gas atoms in an intragranular bubble, n, can be calculated as:

$$n = \frac{f_{ig} C_{gig}}{C_{igb}} \qquad (7\text{-}12)$$

Replacing n in Equation (7-11) by the right-hand side of Equation (7-12), a third-order equation for the bubble radius, r_b, is obtained, as follows:

$$r_b^3 + \frac{2\gamma}{\sigma_h} r_b^2 - \frac{f_{ig} C_{gig}}{C_{igb}} \frac{3kT}{4\pi\sigma_h} = 0 \quad (7\text{-}13)$$

A similar third-order equation was obtained for the intergranular bubble radius and the same solver is used to derive the solution of Equation 7-13.

Once the average intragranular bubble radius that is in mechanical equilibrium with the current thermal-mechanical state of the fuel matrix is calculated from the equation above, the intragranular gaseous swelling, V_{igs}, can be calculated as the volume of all intragranular bubbles, resulting in:

$$V_{igs} = C_{igb} \frac{4\pi r_b^3}{3} \quad (7\text{-}14)$$

[

]

The intragranular gaseous swelling is negligible for standard UO_2 but becomes significant for chromia-doped fuel and is manifested in larger diametral strain increment during power ramps and reduced creepdown during steady-state irradiation. The existing database of the above two parameters for chromia-doped fuel irradiated in both BWR and PWR reactors and a variety of cladding materials allows the calibration of the intragranular gaseous swelling described above. The model parameters f_{ig} and C_{gig} were parametrically varied to arrive at a best-estimate prediction of both creepdown and transient delta strain.

The creepdown data are represented by negative diameter changes, while the deformation increments during power ramps are represented by positive diameter changes. The outward creep can be either positive or negative depending on exposure (i.e. only at high exposures can the clad diameter deformation reversal reach positive numbers).

The results displayed in Figure 7-10 show that all three cladding deformation stages are equally well predicted, demonstrating consistent cladding modeling with the previous database. This provides the basis for qualifying the new intragranular gaseous swelling model for chromia-doped fuel, which drives the diameter change during power ramps and outward creep.

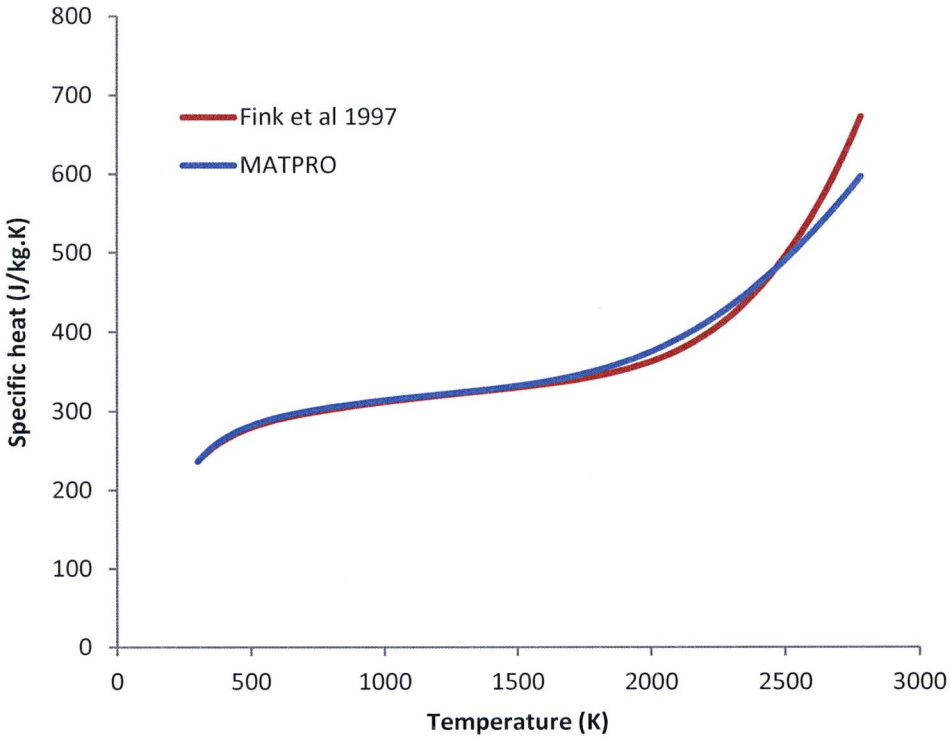

Figure 7-1 MATPRO and Fink Specific Heat Correlations

[

]

Figure 7-2 Re-evaluation of JRC-ITU 1999 Standard UO_2 Diffusivity Data with Consistent Specific Heat Correlation

[

]

Figure 7-3 Diffusivity Measured Data vs Predicted RODEX4 Values for Non-Doped Standard UO_2

[

]

Figure 7-4 Thermal Resistivity for Different Chromia Concentrations

[

]

Figure 7-5 Chromia-Doped RODEX4 Model

[

]

Figure 7-6 Calculated vs Measured Temperatures in the REMORA2 Test

[

]

Figure 7-7 Calculated and Measured Temperatures vs Linear Power in the REMORA2 Test

[

]

Figure 7-8 Fission Gas Release Measured vs Calculated for Chromia-Doped Database

[

]

Figure 7-9 Illustration of Intragranular Porosity Developing in Chromia-Doped Fuel

[

]

Figure 7-10 Strain and Strain Increment Measured vs Calculated for Chromia-Doped Database

8.0 QUALIFICATION OF AURORA-B TO CHROMIA-DOPED FUEL

AURORA-B, a comprehensive evaluation model including the use of both RODEX4 and S-RELAP5 codes, was developed by AREVA for predicting the dynamic response of BWR fuel during transient, postulated accident, and beyond design-basis accident scenarios. RODEX4 provides the realistic evaluation of local thermal-mechanical behavior of fuel rods during such events and S-RELAP5 provides the transient thermal-hydraulic response. The RODEX4 thermal conductivity models for chromia-doped UO_2 and UO_2-Gd_2O_3 are incorporated directly into S-RELAP5 and evaluated for steady state agreement with RODEX4. As summarized in Section 7.1, the thermal conductivity model is evaluated as a function of local temperature, fuel porosity, local burnup, gadolinium fraction and plutonium fraction.

The AURORA-B evaluation model is documented in three separate topical reports: anticipated operational occurrences (AOO) (Reference 25), loss-of-coolant accidents (LOCA) (Reference 26), and control rod drop accidents (CRDA) (Reference 27). Section 9.2 summarizes the AURORA-B sample problems which demonstrate the three AURORA-B methodologies.

9.0 LICENSING CRITERIA ASSESSMENT

Sections 7.0 and 8.0 described the adaptation and qualification of the RODEX4 and S-RELAP5 codes for application to chromia-doped fuel. Both codes have an input parameter to identify the fuel type which will turn on the chromia-doped models when selected.

There is no fundamental change needed for the thermal-mechanical realistic methodology for RODEX4 (Reference 20), or for the three AURORA-B BWR methodologies associated with S-RELAP5 (References 25, 26, and 27). There is also no change to any of the design or licensing criteria.

The following sub-sections illustrate examples of design analyses performed with the chromia-doped fuel option activated in the RODEX4 and S-RELAP5 codes. The results of those analyses are compared to standard fuel analyses to evaluate the impacts of the dopant. There is no generic design analysis to present as the methodologies are applied for each reload and cycle of operation in the power reactor.

9.1 *Steady-state and AOO Analyses (Thermal-Mechanical Evaluation)*

The example thermal-mechanical analysis presented in this report is a repeat of a recent ATRIUM™ 10XM reload calculation performed with the RODEX4 fuel code, but in which the chromia-doped model options were activated by specifying the corresponding input parameters in the RODEX4 input file. In addition, since manufacturing statistics from full batch supply of chromia-doped fuel are not available at this time, the following fuel parameters that are needed to represent the chromia-doped fuel specific behavior were included in the modified input files based on the pre-industrialization manufacturing runs:

[

]

The uncertainty ranges of the gas atom diffusion coefficient and thermal conductivity are the same as for standard UO_2. The consistent prediction (same scatter band) of the

chromia-doped and standard UO_2 FGR allows use of the same uncertainty for both fuel types. With regards to the thermal conductivity, the bounding character of the model adaptation for chromia-doped fuel compensates for the reduced dataset.

Besides the model adaptations and changes necessary to represent chromia-doped fuel behavior, the lower melting temperature of chromia-doped fuel is taken into account. As described in Section 5.2 a bounding correction for the chromia-doped fuel was developed as follows:

[ ]

The sample case selected for illustration herein is from the cycle-specific analyses for reactor A23 Cycle 22. The fuel loading for this cycle is comprised entirely of ATRIUM™ 10XM fuel assemblies; thus, there are three batches of fuel assemblies, the first of which were loaded in Cycle 20 and the other two in subsequent 21st and 22nd cycles. As such, the fuel assemblies in this core approximately span the full range of possible exposure for such fuel.

The results of the sample case are presented in Table 9-1 as the difference between the results for the chromia-doped fuel and the results for standard fuel. A discussion of the difference between the results for the chromia-doped fuel and the results for standard fuel is presented in the following.

[

]

[

]

Therefore, the main conclusions of the comparison of the results for the two fuel types show that chromia-doped fuel thermal-mechanical calculations will typically have the following characteristics:

[

]

[

]

The second part of the thermal-mechanical licensing analysis is the calculation of fast AOO setback factors. This involves the setting of power-dependent LHGR reduction factors (LHGRFACp) for the peak pellet power versus peak pellet exposure-dependent Fuel Design Limit (FDL) as needed to ensure the AOO licensing criteria are met. The criteria addressed in this section are presented in Section 3.1.2 of the RODEX4 methodology (Reference 20):

- The clad tangential uniform transient strain, elastic plus inelastic, shall not exceed 1%.

- Pellet temperatures during anticipated transients shall be maintained below melting.

For AOOs evaluated with the RODEX4 thermal transient solution, the most limiting rod at the FDL or setback fraction of the FDL must not exceed the transient design criteria with 95% probability and 95% confidence.

The fast AOO sample analysis is based on the same ATRIUM™ 10XM fuel case as used in the steady-state sample analysis. Like in the steady-state analysis, the reload calculations were repeated with the chromia-doped option activated in RODEX4. The analysis included comparisons of results between standard UO_2 and chromia-doped UO_2 fuel rods and also between standard gadolinia and chromia-doped gadolinia fuel rods. It is recalled that chromia doping has no impact on the thermal conductivity of gadolinia fuel (Section 4.5), and also that the resintering of the chromia-doped and standard gadolinia fuels are similar. The comparison of the chromia-doped and standard gadolinia results is most relevant because the gadolinia fuel is limiting for fast AOO analysis.

The results of the fast AOO setback sample cases are presented in Table 9-2 for UO_2 fuel and in Table 9-3 for gadolinia fuel. The results illustrate the following impact of chromia-doped fuel rods on the fast AOO setback analysis:

[

]

[

]

9.2 *Safety Analyses*

This section will summarize sample problems performed for three distinct domains: AOO, LOCA, and CRDA. The AOO transient analyses performed with AURORA-B evaluation model is distinct from the AOO transient analysis performed with the stand-alone RODEX4 code (Section 9.1) and is primarily intended to evaluate thermal-hydraulic effects rather than fuel rod mechanical response. Unlike the steady-state and AOO evaluations described in Section 9.1, the AURORA-B methodologies have not yet been licensed. Representative sample problems similar to those presented in the AURORA-B topical reports (References 25, 26, and 27) were performed to illustrate the impacts of chromia-doped fuel on safety analyses.

Two principal effects associated with chromia-doping of fuel pellets result in small impacts to BWR transients and accidents:

- Chromia-doping increases fuel gaseous swelling thereby reducing gap width, which results in increasing gap conductance, increasing overall fuel rod heat transfer to the coolant and decreasing steady state fuel temperature and initial fuel stored energy.

- Chromia-doping decreases fuel thermal conductivity, especially in the low temperature range, thereby reducing the transfer of heat from the interior of the fuel pellet to the pellet surface, which results in reducing overall fuel rod heat transfer to the coolant and increasing steady state fuel temperature and initial fuel stored energy.

These are competing effects in terms of heat transfer to the coolant and initial stored energy which contributes to the magnitude of impacts on transients and accidents. The discussion in Section 7.1 describes both bounding and best-estimate thermal-conductivity correlations in RODEX4.

The application of the best-estimate (upper-bound) correlation is utilized in the AOO methodology to ensure conservatism by increasing the heat transfer to the fluid which would bring the fuel rod closer to boiling transition. Use of the lower bounding curve is conservative in the LOCA and CRDA domains as it increases the steady state fuel temperature and initial fuel stored energy.

Included in the evaluation of chromia-doped fuel were two transients at the end of cycle; a feedwater controller failure (FWCF) and a turbine trip no bypass (TTNB) to evaluate the impacts of ΔCPR, as well as an anticipated transient without scram (ATWS) event to evaluate the impact on peak pressure. The evaluation of LOCA impacts included both small and large break comparisons. The final sample problem includes an evaluation of chromia-doped fuel for a CRDA.

In the transient test cases, ΔCPR is reduced by chromia-doping, indicating that the fuel thermal conductivity effect is more influential than pellet swelling in these test cases. Heat is transferred more slowly to the coolant during the transient, resulting in less thinning of the coolant film at the clad surface. The reduced gap width due to chromia-doping plays an insignificant role at the end of cycle because the gap is nearly closed at the start of the transient, and the temperature drop across the gap is only a small fraction of the total fuel centerline-to-clad-surface temperature drop. The effect of chromia-doping on maximum system pressure is seen to be negligible for all three transient test cases. Table 9-4 summarizes the transient evaluation results.

In contrast to the AOO evaluation, the BWR LOCA test cases indicate that the impact of chromia-doping on LOCA PCT is primarily due to its effect on initial stored energy, which is more influential on large breaks than small breaks. The use of chromia-doping decreases fuel pellet thermal conductivity, leading to increased initial stored energy. The small break case shows no significant change in PCT since it occurs later in the

transient when most of the initial stored energy has dissipated. The clad surface heat transfer rate and PCT are essentially determined by decay heat, minimizing the PCT impact of initial stored energy due to chromia-doping.

The large break case shows a larger increase in PCT because the PCT occurs earlier such that a portion of the initial stored energy still remains and contributes in a small way to the clad surface heat transfer rate, resulting in a slightly increased PCT when chromia-doping is used. For these LOCA test cases, the effect of chromia-doping on PCT is similar to the effect that occurs when gadolinium doping is used, also resulting in reduced fuel thermal conductivity and increased initial stored energy. Table 9-4 summarizes the LOCA evaluation results.

This CRDA test case shows the results of a BWR control rod drop accident. The increase in initial stored energy associated with chromia-doping resulted in an insignificant increase in both the peak channel enthalpy rise and the average enthalpy rise for all modeled channels. Table 9-4 summarizes the CRDA evaluation results.

9.3 *Impact on Nuclear Design Requirements*

There is no impact on reactor physics calculations because chromium and oxygen cross sections are included in the nuclear data library of the CASMO-4 lattice code. Additions of Cr_2O_3 to the fuel will require no changes to existing neutronics codes or methodologies.

The absorption cross section of the chromium additive (3.1 barn) is very small in comparison to that of the fuel. Moreover, the chromium atoms occupy mostly interstitial position in the UO_2 lattice, which is therefore practically not disturbed, resulting in the reactivity coefficients of the chromia-doped fuel being unchanged in comparison to standard fuel.

The requirements of both GDC 11 and GDC 26 regarding the reactivity coefficients of the fuel and the capability of the reactivity control system to maintain the reactor subcritical under cold conditions in situations that include equipment malfunctions, will be satisfied by the specific reload analyses that will be performed for chromia-doped

fuel. These calculations will account for the very small decrease in fuel density for the chromia-doped fuel, which has a small impact on control rod worth in cold conditions.

9.4 *Licensing Criteria Conclusion*

The general conclusions of the sample cases presented above are:

- Some reduction of margin for a few criteria, but margins remain adequate:
    - strain increment, centerline temperature
- Some criteria show margin improvement:
    - internal rod pressure, ΔCPR

Overall, representative sample cases have been selected and analyzed; the results of the analyses are as expected given the performance of chromia-doped fuel.

Table 9-1 Chromia-Doped Thermal-Mechanical Analysis Sample Case Results

[

]

[

]

Table 9-2 Fast AOO Sample Case Comparing Chromia-Doped UO_2 Fuel and Non-Doped UO_2 Fuel Analyses

[

]

Table 9-3 Fast AOO Sample Case Comparing Chromia-Doped GAD Fuel and Non-Doped GAD Fuel Analyses

[

]

Table 9-4 Impact of Chromia-Doping on BWR Sample Test Cases

[

]

10.0 OPERATING EXPERIENCE

Since 1997, chromia-doped fuel rods and LFA's (Lead Fuel Assemblies) of various AREVA designs have been irradiated in commercial PWR and BWR reactors. No problems have been reported from the plants which are related to the doped fuel. Today, the experimental database covers chromia-doped UO_2 fuel pellets enriched up to 4.95% U^{235} [

].

10.1 *Steady State Irradiation*

Chromia-doped fuel has been irradiated in PWR and BWR power reactors since 1997, as follows:

- A total of [ ] irradiation campaigns have hosted or are hosting chromia-doped fuel rods and LFAs equipped with chromia-doped pellets. Behavior has been as expected with a maximum rod burnup of approximately [ ].
- An LFA program in a U.S. BWR is nearing completion. The fuel will reach end-of-life exposures and be discharged after six years of operation in 2017.

The main characteristics of the irradiation campaigns outlined above are summarized in Table 10-1.

10.2 *Ramp Testing and Demonstrated PCI Benefit of Chromia-doped Fuel*

The PCI performance of the chromia-doped UO_2 fuel was determined through dedicated and comprehensive power ramp test programs for both PWR and BWR applications (summarized in Section 6.2), which allowed the assessment of PCI performance gains relative to standard UO_2. In both PWR and BWR cases, the fuel and ramp test

parameters were selected such that the potential of failure risk is maximized with respect to the PCI mechanism involved.

To provide the most limiting conditions for the ramp tests, most of the power-ramped fuel rods were base-irradiated to an exposure in the [ ], which is the most critical for PCI failures. At higher exposures, the fuel has been shown to be less sensitive to the PCI type of failure mechanism. However hydrogen induced failure is a potential additional concern for very high exposure fuel. Therefore, in order to obtain a comprehensive assessment of chromia-doped UO_2 fuel, the power ramp program also included very high burn-up fuel.

Studies were done to analyze the power ramp databases with doped and standard fuels in order to derive relevant PCI failure thresholds. Historically, thresholds were derived from power ramp data presented as ramp terminal level versus burn-up. However, this formulation does not capture the initial power effect which reflects the degree of fuel rod deconditioning that can occur in operation. No clear segregation between failed and non-failed rods is observed with this formulation (Reference 28).

In another approach, the power increment (ΔP) was shown (Reference 29) to be a determining parameter to derive a best-estimate failure threshold from the power ramp database, which is inversely proportional to initial power (P_i). This ΔP - P_i threshold has a burn-up dependency, which saturates in the mid-burnup range and can be conservatively applied for lower burn-up values. The ΔP - P_i criterion was demonstrated on the historical power ramp database (Reference 29) and also on recent power ramp programs that use modern fuel. According to this $\Delta P - P_i$ correlation, the chromia-doped fuel BWR ramp results are presented in Figure 10-1 together with the old non-liner standard fuel failure PCI threshold and the more recent liner rods. In the same figure, PWR data with chromia-doped fuel are included showing a consistent behavior with the BWR data. The fuel rod design and base irradiation conditions mainly affect the susceptibility of the test rod to fail by PCI. Assuming equivalent degree of conditioning of the tested BWR and PWR chromia-doped fuel rods, the failure threshold

and PCI resistance is mainly affected by ramp parameters controlling the cladding stress in the ramp.

The main conclusions that can be derived from the comparison of chromia-doped fuel with standard fuel power ramp data are as follows (Reference 30):

- For BWR applications, the chromia-doped PCI failure threshold brings benefits in comparison not only with the historical database, but more importantly with respect to modern liner fuel, especially in the range of medium high initial power levels. In that case, the benefit is a gain in margin of 7 to 10 kW/m (power increment) in comparison to the standard liner or non-liner fuel threshold (Reference 31).

- For PWR applications, the chromia-doped rods show a power increment failure that is 4 kW/m higher than for standard UO_2 M5™ fuel rods (Reference 32).

The chromia-doped fuel PCI failure threshold has been well defined by the PWR and BWR ramp programs. In particular, the degree to which the behavior of this fuel is enhanced with respect to standard UO_2 allows considering the chromia-doped fuel as an alternative to the present liner cladding in terms of PCI protection for BWR applications.

Table 10-1 Operating Experience with Chromia-doped Fuel

[

]

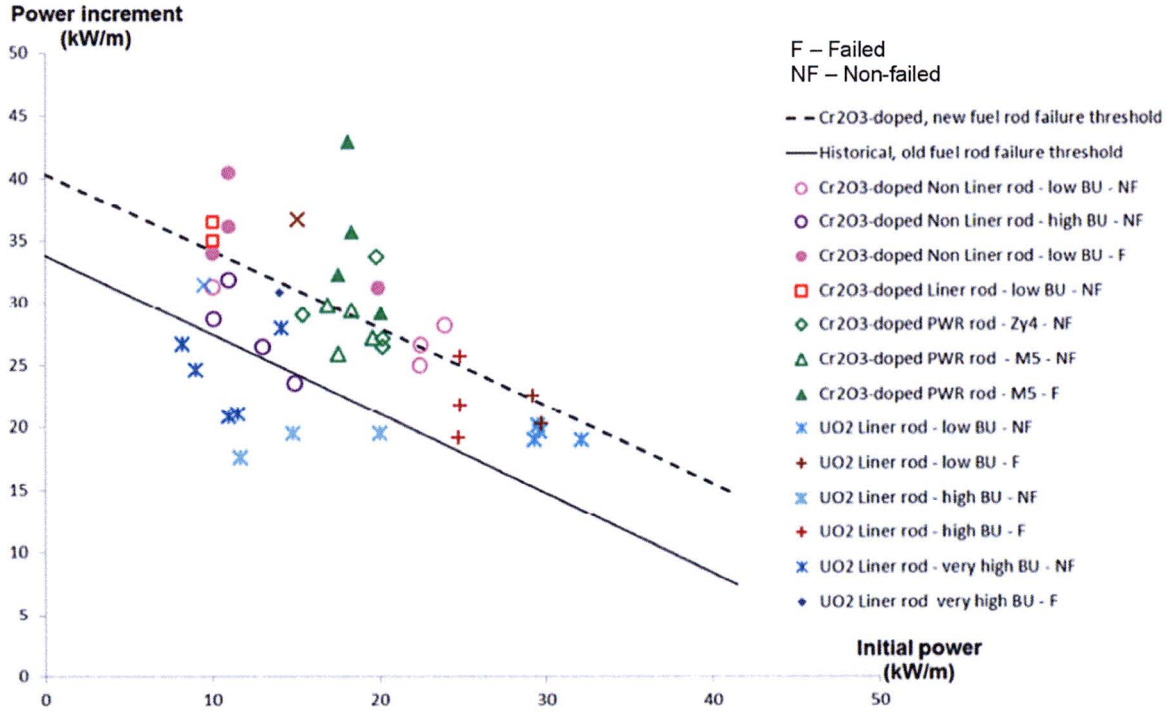

Figure 10-1 Ramp Test Data Showing Increased Fuel Failure Threshold for Chromia-Doped Fuel

11.0 REFERENCES

1. Standard Review Plan, NUREG-0800, Chapter 4, U.S. Nuclear Regulatory Commission, March 2007.

2. J. C. Killeen, "Fission gas release and swelling in UO2 doped with Cr2O3", Journal of Nuclear Materials, Vol. 88 (1980), pp. 177-184.

3. A. Leenaers, L. de Tollenaere, Ch. Delafoy, S. Van den Berghe, "On the solubility of chromium sesquioxide in uranium dioxide fuel," Journal of Nuclear Materials 317 (2003) 62–68.

4. A.C. Momin et al, "High temperature X-ray diffractometric studies on the lattice thermal expansion behavior of UO2, ThO2 and (U0.2 Th0.8)O2 doped with fission product oxides," Journal of Nuclear Materials, Volume 185, (1991), Pages 308-310.

5. J. A. Cape, G. W. Lehman, "Temperature and finite pulse-time effects in the flash method for measuring thermal diffusivity," Journal of Applied Physics, Vol. 34, No. 7, 1963 pp. 1909-1913.

6. E 1461 – 01, "Standard test method for thermal diffusivity by the flash method," Annual Book of ASTM Standards, 2001.

7. C. Ronchi, M. Sheindlin, M. Musella and G.J. Hyland, "Thermal conductivity of uranium dioxide up to 2900 K from simultaneous measurement of the heat capacity and thermal diffusivity," Journal of Applied Physics, vol 85, number 2, 15 January 1999, p. 776.

8. MATPRO NUREG/CR-6150, Vol. 4, Rev. 2, INEL-96/0422 SCDAP/RELAP5/MOD 3.3 Code Manual, MATPRO – A library of Material Properties for Light-Water-Reactor Accident Analysis.

9. D.G. Martin, "The elastic constants of polycrystalline UO_2 and $(U,Pu)O_2$ mixed oxides – A Review," High Temperatures - High Pressures, Volume 21, 1989.

10. A. G. Evans and R.W. Davidge, "The strength and fracture of stoichiometric polycrystalline UO_2," Journal of Nuclear Material, Volume 33, (1969), pp 249-260.

11. M. Oguma, "Microstructure effects on fracture strength of UO_2 fuel pellets," Journal of Nuclear Science and Technology, Volume 19, Number 12, (1982) pp 1005-1014.

12. F. Lemoine, D. Baron and P. Blanpain, "Key parameters for the High Burnup Structure formation thresholds in oxide fuels," Proceedings of 2010 LWR Fuel Performance/TopFuel/WRFPM Orlando, Florida, September 26-29, (2010), Paper 062.

13. K. Nogita et al, "Effect of grain size on recrystallization in high burnup fuel pellets," Journal of Nuclear Materials, Vol. 248 (1997), pp. 196-203.

14. K. Une and S. Kashibe, "Corrosion behavior of irradiated oxide fuel pellets in high temperature water," Journal of Nuclear Materials, Vol. 232 Issues 2-3 (1996), pp. 240-247.

15. D. Manara et al, "Thermophysical measurements for AREVA Gd and Cr doped UO2," Report JRC96692, JRC-ITU, 2015.

16. D. Manara, M. Sheindlin, W. Heinz, and C. Ronchi, "New techniques for high-temperature melting measurements in volatile refractory materials via laser surface heating," Rev. Sci. Instrum.," 79 (2008) p. 113901.

17. R. Böhler, M.J. Welland, D. Prieur, P. Cakir, T. Vitova, et al., "Recent advances in the study of the UO2–PuO2 phase diagram at high temperatures," J. Nucl. Mater. 448 (2014) pp 330-339.

18. A. Puranen et al. "Burnup effects on fine fuel fragmentation in simulated LOCA testing," Proceedings of the LWR Fuel Performance Meeting TopFuel 2013, Charlotte, NC, September 15-19, (2013).

19. F. Lemoine, "High burnup fuel behavior related to fission gas effects under reactivity-initiated accident (RIA) conditions," Journal of Nuclear Materials, Volume 248, (1997), Pages 238-248.

20. BAW-10247-PA Revision 0, "Realistic Thermal-Mechanical Fuel Rod Methodology for Boiling Water Reactors," AREVA NP, February 2008.

21. "Thermophysical properties database of materials for light water reactors and heavy water reactors," IAEA-TECDOC-1496, IAEA, June 2006.

22. J. K. Fink and M. C. Petri, "Thermophysical properties of Uranium Dioxide," ANL/RE-97/2, February 1997.

23. R. J. White, "The Growth of intra-granular bubbles in post-irradiation annealed UO_2 Fuel," in "Nuclear fuel behavior modelling at high burnup and its experimental support" Proceedings of a Technical Committee meeting held in Windermere, United Kingdom, 19-23 June 2000.

24. R. J. White, "Fission Gas Release," HWR-632, Halden 2000.

25. ANP-10300P Revision 0, "AURORA-B: An Evaluation Model for Boiling Water Reactors; Application to Transient and Accident Scenarios," AREVA NP, December 2009.

26. ANP-10332P Revision 0, "AURORA-B: An Evaluation Model for Boiling Water Reactors; Application to Loss of Coolant Accident Scenarios," AREVA, February 2014.

27. ANP-10333P Revision 0, "AURORA-B: An Evaluation Model for Boiling Water Reactors; Application to Control Rod Drop Accident (CRDA)," AREVA, March 2014.

28. M. Billaux, "Modeling pellet-cladding mechanical interaction and application to BWR maneuvering," Proceedings of the 2004 International Meeting on LWR Fuel Performance. Orlando, Florida, September 19-22, 2004.

29. B. Cox. Pellet-clad interaction (PCI) failures of zirconium alloy fuel cladding – A review. Journal of Nuclear Materials Vol. 172, Issue 3 (1990), pp. 249 – 292.

30. C. Delafoy, V.I. Arimescu, R.M. Hengstler-Eger, H. Landskron, A. Moeckel, "AREVA Cr_2O_3-doped Fuel: Increase in Operational Flexibility and Licensing Margins," Topfuel, Zurich, September 13-17, 2015.

31. P. B. Hoffmann, P. Dewes. Post-irradiation examination and ramp testing of fuel rods with Fe-enhanced Zr liner cladding at high burnup. Proceedings of the 2004 International Meeting on LWR Fuel Performance. Orlando, Florida, September 19-22, 2004.

32. N. Teboul et al. AREVA optimized fuel rods for LWRs. Proceedings of the 2012 TopFuel Reactor Fuel Performance meeting, Manchester, United Kingdom, September 2-6, 2012.

33. C. Delafoy, P. Dewes, T. Miles, "AREVA NP Cr_2O_3-Doped Fuel Development for BWRs," Topfuel, San Francisco, September 30-October 3, 2007.